Journal of Nuclear Materials 527 (2019) 151780

Contents lists available at ScienceDirect

Journal of Nuclear Materials

journal homepage: www.elsevier.com/locate/jnucmat

Vaporization behaviour of a PuF_3-containing fuel mixture for the Molten Salt Fast Reactor

A. Tosolin [a, b, *], J.-Y. Colle [a], S. Mastromarino [a, c], P. Souček [a], L. Luzzi [b], R.J.M. Konings [a, c], O. Beneš [a, *]

[a] European Commission, Joint Research Centre, P.O. Box 2340, 76125, Karlsruhe, Germany
[b] Politecnico di Milano, Department of Energy, Via La Masa 34, 20156, Milan, Italy
[c] Delft University of Technology, Department of Radiation Science & Technology, Mekelweg 15 2629 Delft, Netherlands

HIGHLIGHTS

- First partial vapour pressure results on a PuF_3-containing fuel mixture for the Molten Salt Fast Reactor.
- First results on eutectic melting, liquidus and boiling point for the LiF-ThF_4-UF_4-PuF_3 (77.5–6.6-12.3–3.6 mol%) fuel mixture.
- Second independent study on melting point and appearance potential of PuF_3.
- New data on PuF_3 vapour pressure and enthalpy of sublimation.

ARTICLE INFO

Article history:
Received 26 June 2019
Received in revised form
6 August 2019
Accepted 29 August 2019
Available online 30 August 2019

Keywords:
Fluoride fuel
Molten salt reactor
Knudsen effusion mass spectrometry
Vapour pressure
Plutonium trifluoride

ABSTRACT

The mixture LiF-ThF_4-UF_4-PuF_3 (77.5–6.6-12.3–3.6 mol%), a fuel option for the Molten Salt Fast Reactor (MSFR), has been measured by differential scanning calorimetry (DSC) for determination of phase transitions, and by Knudsen effusion mass spectrometry (KEMS) for measurement of partial vapour pressures. The boiling point of the mixture was determined by extrapolation of total vapour pressure to 1 bar. Thermodynamic calculations were performed and compared with the experimental results. Novel experimental data on pure plutonium trifluoride are presented: melting point, vaporization enthalpy, vapour pressure and ionization energies by electron impact.

1. Introduction

The Molten Salt Reactor (MSR) is a nuclear reactor concept in which the thermal carrier and/or the nuclear fuel is a mixture of molten salts (generally chlorides or fluorides). This technology was initially developed around the middle of the last century at Oak Ridge National Laboratory (ORNL) in United States of America for both military [1,2] and civilian applications [3–5], collecting an extensive knowledge on molten salts. Subsequently, the interest and the financial support for this technology strongly reduced [6], as other concepts seemed more appealing.

At the beginning of 2000s, the Generation IV International Forum (GIF) selected the MSR among the six most promising future reactors [7]. Since then, the interests for this concept has been rapidly growing [8]. Nowadays, many MSR concepts are studied worldwide, exploring different sizes, fuels and technical solutions [9].

In this context, a consortium of European partners has been working for the development of a large size MSR, in which a mixture of molten fluorides circulates at ambient pressure in the primary circuit, reaching temperatures close to 1073 K. This concept, named Molten Salt Fast Reactor (MSFR) [10], aims to utilize a closed thorium fuel cycle and a fast neutron spectrum, and it can potentially operate both as breeder and incinerator, with great benefits in terms of safety and sustainability [11,12]. Safety related

* Corresponding authors. European Commission, Joint Research Centre, P.O. Box 2340, 76125, Karlsruhe, Germany.
E-mail addresses: alberto.tosolin@polimi.it (A. Tosolin), Ondrej.BENES@ec.europa.eu (O. Beneš).

https://doi.org/10.1016/j.jnucmat.2019.151780

features of the MSFR are currently under study within the European Horizon2020 project SAMOFAR [13].

The reference MSFR [14] is a 3000 MW_{th} reactor with a fertile blanket around the core, filled with eutectic LiF—ThF_4. The nuclear fuel is dissolved in the coolant, giving a homogenous core and allowing fuel reprocessing and/or clean-up online and continuously [15]. The exact composition of the fuel depends on overall reactor purpose and design (e.g., breeder, incinerator), but must also fulfil considerations about chemistry, neutronics, availability of the fissile materials and desired thermo-chemical and thermo-physical properties. According to the research done so far, a suitable fuel composition for the MSFR is 77.5 mol% of lithium fluoride and 22.5 mol% of actinide fluorides containing both fissile and fertile materials. More in detail, the fissile material can be uranium-233 (obtained from thorium-232), enriched uranium (with enrichment lower than 20% due to proliferation resistance issues), plutonium-239 and minor actinides, or a mix of these solutions [16].

The assessment of safety-related properties of the MSFR fuel options is a crucial issue. In this frame, the experimental research may drive the final selection of the MSFR fuel and give fundamental inputs to the reactor design and operation. Among these properties, the partial vapour pressure vs. temperature of the fuel components is very important as it determines parameters useful for both reactor operation and fuel clean-up.

In our previous work [17], we studied the selected LiF-ThF_4-UF_4 (77.5—20.0-2.5 mol%) fuel composition, suitable for a $^{232}Th/^{233}U$ closed fuel cycle. In that study, we used differential scanning calorimetry (DSC) to determine the melting temperature and Knudsen effusion mass spectrometry (KEMS) to measure the vapour pressure. Since plutonium trifluoride is also under consideration for the MSFR fuel [18], the relevant PuF_3-containing fuel mixture LiF-ThF_4-UF_4-PuF_3 (77.5—6.6-12.3—3.6 mol%) is here studied with the same approach. In order to complement the required data for the end-members already measured in our previous works [17,19], new data for the melting point and the vapour pressure of pure PuF_3 are presented in this study as well.

2. Experimental

2.1. Initial materials

LiF with metal base purity of 99.99% was purchased from Alfa Aesar. Actinide fluorides were synthetized by hydrofluorination of respective oxides, which were obtained from nitrates dropped in oxalic acid and subsequent calcination of the oxalates. As the products of the hydrofluorination of ThO_2, UO_2 and PuO_2 are ThF_4, UF_4 and PuF_4, respectively, PuF_4 was then reduced to PuF_3 by hydrogenation. For details about the synthesis of these end-members, we refer to our previous works [20,21].

Because these fluorides are very hygroscopic and sensitive to oxygen [22,23], they were handled and stored in argon glove boxes in which the content of oxygen and moisture is continuously monitored and kept below a few ppm.

Before the preparation of the samples, lithium fluoride was purified according to a process consisting in heating up to 673 K for 4 h to evaporate possible residual water. Then, the purity of all the end-members was assessed by DSC. According to this procedure, the material is considered pure if the DSC outcome gives one clear peak in correspondence of the melting point, as determined in our previous work [20].

The LiF-ThF_4-UF_4-PuF_3 (77.5—6.6-12.3—3.6 mol%) mixture was prepared mixing the end-members in an agate mortar.

2.2. Differential scanning calorimetry

The measurements were performed with a Setaram multi-detector high temperature calorimeter (MHTC 96) equipped with a DSC sensor and B-type thermocouple, allowing measurements up to 1873 K. The instrument is installed inside an argon glove box and connected to a helium line. Because fluoride vapours are chemically aggressive and may damage the internal parts of the device, the sample was encapsulated in a stainless steel crucible with an internal nickel liner for chemical compatibility [24]. Details about the encapsulation technique are described in our previous work [25].

Prior to the measurements, the experimental chamber was purged and evacuated twice up to a few pascals to eliminate possible impurities. A first heating ramp was performed to melt the mixture and assure a complete mixing of the end-members. The maximum temperature was 1473 K, which is above the expected liquidus point. The eutectic melting of LiF-ThF_3-UF_4-PuF_3 (77.5—6.6-12.3—3.6 mol%) was measured from the second heating ramp, taking the onset point of the peak formed on the DSC heat flow signal. The liquidus temperature of the fuel mixture was determined from the change of slope in the DSC heat flow curve. Heating ramps were performed at 10 K/min, 5 K/min and 2 K/min to assess repeatability. The measured temperatures were corrected to ITS-90 by the calibration of our device, with certified calibration materials (Al, Sn, Ag, In, Pb, Au) at different heating rates.

2.3. Knudsen effusion mass spectrometry

The KEMS device [26] is installed inside a nitrogen glove box with additional lead shields. It consists of 21 mm high Knudsen cylindrical cell (a cell with a 0.5 mm diameter orifice at the top), surrounded by a heating element and thermal shields. The cell is made of tungsten and the temperature inside is monitored by a pyrometer focused at the black body hole at the bottom part of the cell.

The experiment was done under vacuum at a pressure below 10^{-4} Pa to avoid interaction between the sample and the atmosphere. Upon heating, vapour molecules escape from the orifice. If the orifice diameter is smaller than the mean free path of the vapour molecules in the cell (Knudsen flow regime), we can assume that the system remains in equilibrium. As long as this condition remains, the number of molecules of a certain species escaping from the orifice is proportional to its partial vapour pressure. Vapour molecules are detected by a quadrupole mass spectrometer (MS) equipped with a cross beam electron source and a secondary electron multiplier (SEM). For details about the KEMS technique, we refer to comprehensive reviews published in literature [27,28].

The electron energy was set at 32.85 eV. For measuring the appearance potential of the ions from the PuF_3 neutral precursor, it was increased from 0 to 42 eV, maintaining a constant temperature of 1469 K, high enough to have clear signal of all gaseous species.

To get the vapour pressure values, the MS signal must be analysed considering the ionization cross sections of all species in the vapour. All different isotopic compositions were taken into account. Furthermore, fragmentation may occur after the ionization, so that different ionic species may result from the same neutral precursor.

In the ideal case of only mono-isotopic species and no fragmentation prior to ionization, the relation between the MS signal of a species i and its partial vapour pressure p_i is:

$$p_i = K_i \cdot T \cdot I_i^+ \tag{1}$$

in which T is the temperature, I_i^+ is the MS signal of the i species, and K_i is a coefficient of proportionality. K_i depends on many factors such as the geometry and the efficiency of the device, the ionization

cross section of the species *i*, and the SEM gain. The contribution to K_i due to the geometry and the efficiency of the KEMS device was determined putting a small piece of a reference material together with the sample. In this work, silver and nickel were used as reference materials for the mixture LiF-ThF_4-UF_4-PuF_3 (77.5–6.6-12.3–3.6 mol%) and for PuF_3, respectively. The calibration materials were selected to avoid chemical reactions with the samples and to have significant signal in the temperature range at which also the samples evaporate, in order to perform calibration in similar conditions. The MS signal I^+_{ref} is related to the vapour pressure of the reference material p_{ref} [29] through the following relation:

$$K_{ref} = \frac{p_{ref}}{I^+_{ref} \cdot T} \tag{2}$$

The contributions to K_i due to the ionization cross section and the SEM gain of the species *i* are normalized to the reference material:

$$K_i = K_{ref} \frac{\gamma_i}{\gamma_{ref}} \frac{\sigma_{ref}}{\sigma_i} \tag{3}$$

in which the ratios γ_i / γ_{ref} and σ_{ref} / σ_i are the normalized SEM gain and the normalized ionization cross section, respectively. As suggested by Grimley [30], the SEM gain is proportional to the square root of the mass of the ion. This is generally a good approximation for molar masses higher than 50 amu. In this case, equation (3) can be written as:

$$K_i = K_{ref} \frac{\sqrt{M_i}}{\sqrt{M_{ref}}} \frac{\sigma_{ref}}{\sigma_i} \tag{4}$$

which is valid for all ions coming from actinide neutral precursors considered in this study (ThF_4, UF_4, PuF_3). Since ions from lithium species have generally masses lower than 50 amu, values of γ_i / γ_{ref} suggested by Yamawaki et al. [31] were used. Similarly to us, they performed KEMS experiments on LiF using silver as calibration material, identifying Li^+, LiF^+, Li_2F^+ and $Li_3F_2^+$ as the main ionic species coming from electronic bombardment of LiF vapour species, which evaporates in form of monomer LiF, dimer Li_2F_2 and trimer Li_3F_3. They suggested normalized SEM gains γ_i / γ_{ref} of 0.87, 1.47, 1.66 and 2.48, for Li^+, LiF^+, Li_2F^+ and $Li_3F_2^+$, respectively.

Normalized ionization cross sections of vapour lithium species were taken from Yamawaki et al. [31] as they performed their experiment in very similar conditions, using a 30 eV electron beam. The Ionization cross sections of nickel and silver, used as reference materials, were taken from Mann [32]. Due to the lack of experimental data, for the determination of the ionization cross sections of AB_n-type molecules (ThF_4, UF_4 and PuF_3), the modified additivity rule by Deutsch et al. [33] was applied, which is defined as:

$$\sigma(AB_n) = \left[\frac{r_A^2}{r_B^2}\right]^{\alpha} \left[\frac{\xi_A}{\xi_A + n\xi_B}\right] \sigma_A + \left[\frac{nr_B^2}{r_A^2}\right]^{\beta} \left[\frac{n\xi_B}{\xi_A + n\xi_B}\right] n\sigma_B \tag{5}$$

in which r_A, r_B and ξ_A, ξ_B refer to the atomic radii and the effective number of electrons of the constituent atoms A and B, respectively. Their values are taken from the tables of Desclaux [34]. The superscript α and β are determined according to an empirical relation described in detail in their paper [33]. The authors compared several calculations with available experimental data (generally affected by an uncertainty of 15–20%) quoting error margins of 15–25%. Values for ThF_4 and UF_4 were calculated in our previous work according to this method, while ionization cross section for PuF_3 was calculated in this work. Ionization cross sections used in this study are listed in Table 1.

If fragmentation occurs prior to ionization, equations (3) and (4) should be re-written for each ion *j* coming from a neutral precursor *i*:

$$K_j = K_{ref} \frac{\gamma_j}{\gamma_{ref}} \frac{\sigma_{ref}}{\sigma_i} \tag{6}$$

$$K_j = K_{ref} \frac{\sqrt{M_j}}{\sqrt{M_{ref}}} \frac{\sigma_{ref}}{\sigma_i} \tag{7}$$

The partial vapour pressure of a species *i* is then the sum of all contributions *j* of the ions from the same neutral precursor:

$$p_i = \sum_j K_j \cdot T \cdot I_j^+ \tag{8}$$

with appropriate corrections to consider isotopes and their possible combinations in a molecule (e.g., $^6Li^7LiF_2$).

If during the KEMS measurement the sample changes from solid to liquid phase, the mass spectrometric signal generally indicates a change of slope or a plateau. This technique was used to estimate the melting temperature of PuF_3. We note that measuring melting temperature by this approach is typically less reliable than measuring this quantity by DSC, because the temperature read by the pyrometer may be affected by the window in optical path of the laser, increasing the uncertainty. However, liquid transition of PuF_3 was not measured by DSC in this work, due to its high melting point and the unavailability of a suitable encapsulation.

3. Results and discussion

3.1. Phase transitions

The DSC curve obtained at 10 K/min for the mixture LiF-ThF_4-UF_4-PuF_3 (77.5–6.6-12.3–3.6 mol%) is shown if Fig. 1.

The onset of the first clear peak indicates the eutectic melting, while the offset of the second broad peak indicates the liquidus point. The analysis of the DSC curves gives 776 ± 3 K and 893 ± 10 K for the eutectic and liquidus points, respectively. Given uncertainties are based on the experience and the literature [35], which suggests to use a larger error for the liquidus point as the signal is less clear. Both transitions were calculated using the thermodynamic database assessed by Capelli et al. [36] in combination with the FactSage thermodynamic software [37]. A visual representation of the calculations is given in Fig. 2, in which the pseudo binary LiF-ThF_4-UF_4-PuF_3 phase diagram with a fixed amount of ThF_4 (6.6 mol%) and PuF_3 (3.6 mol%) is shown together with the experimental points obtained by DSC.

The calculated liquidus temperature is about 40 K lower than the experimental one, which might seem a significant difference.

Table 1
Cross section values used in this work.

Species *i*	σ_i [10^{-16} cm^2]	Reference
Ag	5.0458	[32]
Ni	5.4506	[32]
LiF	3.0779	[31]
Li_2F_2	3.5825	[31]
Li_3F_3	4.2889	[31]
ThF_4	8.9184	[19]
UF_4	8.8879	[17]
PuF_3	9.7911	This work

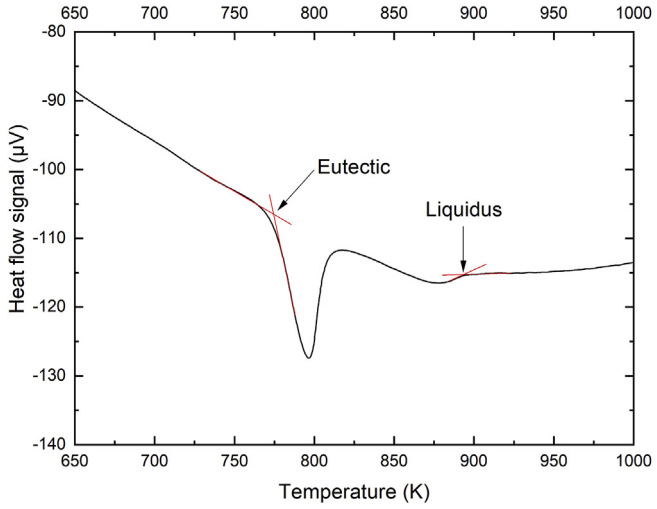

Fig. 1. DSC curve of the mixture LiF-ThF_4-UF_4-PuF_3 (77.5–6.6-12.3–3.6 mol%) during the heating at 10 K/min.

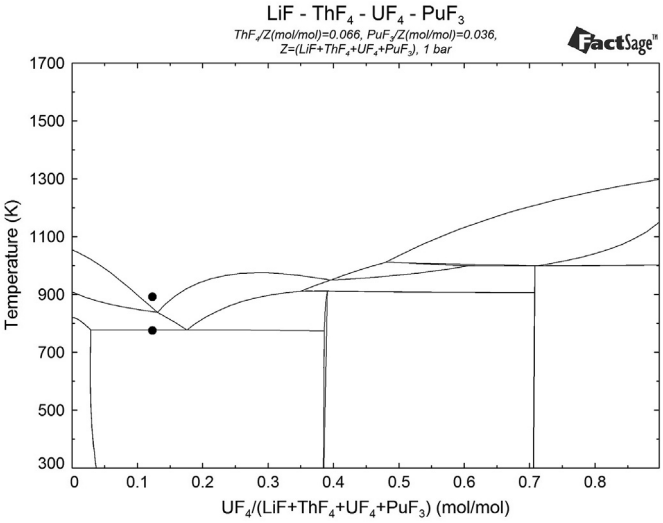

Fig. 2. The LiF-ThF_4-UF_4-PuF_3 phase diagram for fixed amounts of ThF_4 and PuF_3 of 6.6 and 3.6 mol% respectively. Black circles represent experimental points obtained by DSC.

However, the point is very close to the relatively steep liquidus and, in this region, a melting temperature shift of 40 K corresponds to a change of 1.5 mol% composition towards LiF, which is slightly above the experimental uncertainty of the composition of ±1.0 mol%. Alternatively, the observation may suggest that a slight correction in the thermodynamic database is needed.

3.2. Vapour pressure of plutonium trifluoride

Vapour pressure of PuF_3 was measured from 1310 to 1629 K. The results are listed in Annex Table 1 and graphically represented in Fig. 3. The corresponding vapour pressure equation is obtained by fitting the experimental results to a ln(p) vs. $1/T$ van 't Hoff equation:

$$\ln p(Pa) = -\frac{(45874\pm721)}{T(K)} + (31.290\pm652) \quad (9)$$

Uncertainties for the slope and the quote in equation (9) are

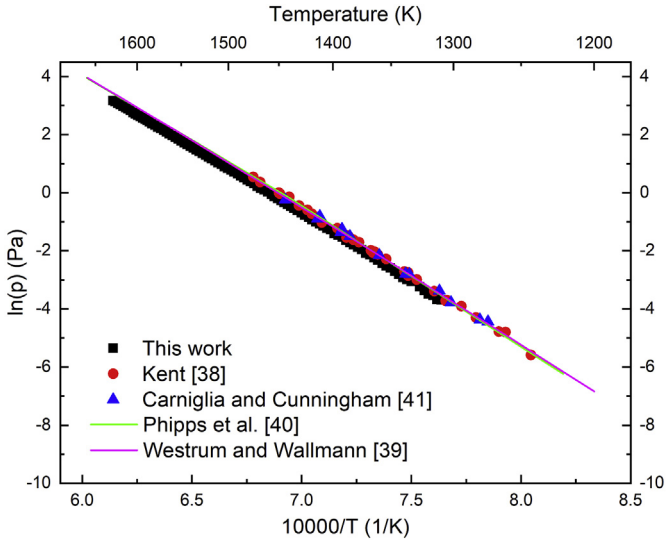

Fig. 3. Vapour pressure trend lines for solid PuF_3 calculated using experimental data of different authors.

determined considering ± 1% uncertainty on the temperature read by the pyrometer (which may be affected by the conditions of the quartz optical window crossed by the laser) and ±20% on the ionization cross sections of the fluoride species, as discussed in Section 2.3.

Fig. 3 also shows the experimental results reported by other authors using mass spectrometry [38] and effusion method [39–41]. Because Westrum and Wallmann [39] did not publish the vapour pressure values and we found inconsistency between the vapour pressure values and equation published by Phipps et al. [40], we show the reported equations for these authors. As shown in Fig. 3, our results are in very good agreement with these studies.

Enthalpy of sublimation was determined from our vapour pressure data, according to the second law method:

$$\Delta H^{\circ}_{Sub,T_M} = -R\frac{d(\ln K_{eq})}{d(1/T)} \quad (10)$$

and the third law method:

$$\Delta H^{\circ}_{Sub,298} = -T\left[R\ln K_{eq} + \Delta\frac{G^{\circ}_T - H^{\circ}_{298}}{T}\right] \quad (11)$$

where T_M is the mean temperature of the measurement, R is the universal gas constant, K_{eq} is the equilibrium constant of the sublimation reaction and $\Delta[(G^{\circ}_T - H^{\circ}_{298})/T]$ is the change of the Gibbs energy function of the reaction considered. The quantity $\ln K_{eq}$ is proportional to the vapour pressure obtained from the measurement, while thermodynamic functions of PuF_3 were taken from literature [42]. The second law approach gives $\Delta H^{\circ}_{1473} = 407\pm2$ kJ·mol^{-1}. The third law approach gives $\Delta H^{\circ}_{298} = 423\pm1$ kJ·mol^{-1}. Given uncertainties represent standard deviations. The value obtained from the third law treatment is in very good agreement with the value of 422.6 ± 12.6 kJ·mol^{-1} suggested by Kent [38]. This quantity was also recalculated using the thermodynamic functions used in this work [42] and vapour pressure measurements by Kent, finding 423 ± 20 kJ·mol^{-1}.

Ionization efficiency curves obtained for the pure PuF_3 precursor are shown in Fig. 4. Energy thresholds are selected by extrapolating the tangents to the zero value of the MS signal, as indicated for the ion PuF_2^+. Fig. 4 also shows the electron energy value of 32.85 eV,

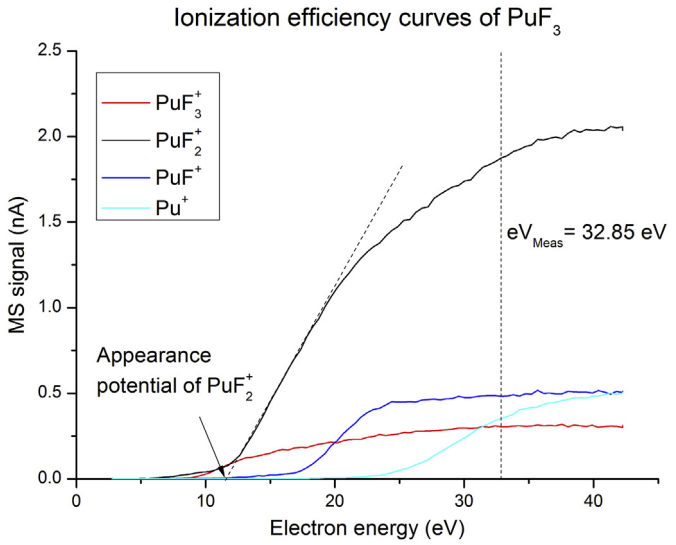

Fig. 4. Ionization efficiency curves from a neutral PuF_3 precursor by electron impact. Selected values correspond to the extrapolation of the tangent to the zero value of the MS signal.

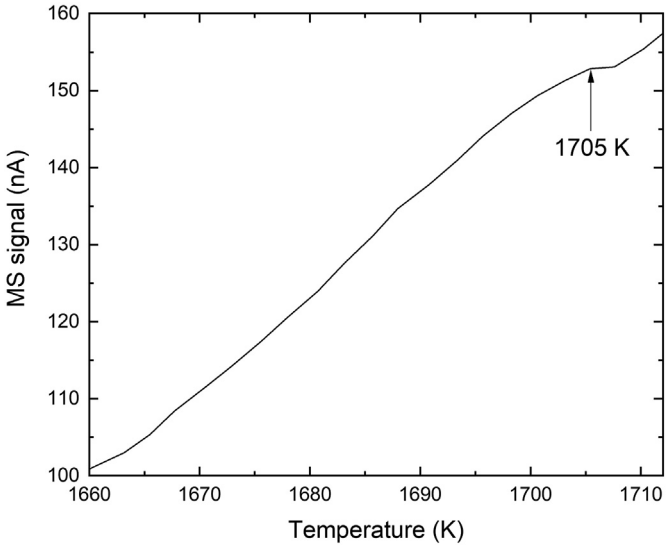

Fig. 6. Detection of PuF_3 melting point by KEMS. The signal shows a marked change of slope.

which was selected during the measurement of the vapour pressure.

The appearance potentials obtained from the measurement are 9.0 ± 1.0 eV for PuF3+, 11.8 ± 1.0 eV for PuF2+, 17.1 ± 1.0 eV for PuF+, and 24.5 ± 1.0 eV for Pu+. These values are graphically represented in Fig. 5.

These measurements were also performed by Kent [38], who reported 12.6 ± 0.5 eV for PuF2+, 18.0 ± 1.0 eV for PuF+, and 25.0 ± 1.0 eV for Pu+ (value for PuF3+ was not reported). These values are in good agreement with ours.

Finally, the melting point of PuF3 was determined from the mass spectrometric signal as 1705 ± 10 K, shown in Fig. 6 as a plateau.

This quantity was previously measured by Westrum and Wallmann [39], using direct observation of the fusion and solidification points with an optical pyrometer, and obtained a value of 1699 ± 3 K. This value must be corrected to the International Temperature Scale of 1990 (ITS-90), giving 1700 ± 3 K, which is just 5 K lower than our measurement.

3.3. *Vapour pressure of LiF-ThF_4-UF_4-PuF_3 (77.5–6.6-12.3-3.6 mol%)*

Partial vapour pressure results obtained by KEMS for the mixture LiF-ThF_4-UF_4-PuF_3 (77.5–6.6-12.3–3.6 mol%) are presented in Annex Table 2 Linear fits on the ln(p) vs. $1/T$ diagram are shown in Fig. 7 as solid lines, and respective equations are listed in Table 2, together with temperature ranges of validity. Uncertainties were determined considering ±1% uncertainty on the temperature read by the pyrometer and ±20% on the ionization cross sections of the fluoride species, as discussed in Section 2.3.

Calculations performed using the thermodynamic assessment presented in the work of Capelli et al. [36] have been compared with partial vapour pressure equations proposed in this work (Fig. 7). The calculations reproduce reasonably well the vaporization behaviour of the main lithium species (LiF and Li_2F_2), as well as UF_4, which agree within one order of magnitude or better. These deviations are acceptable considering these low vapour pressure values. The agreement is less for the other species, but again we should note that the actual pressures are very low. In this regard, we point out that the activities for LiF–ThF_4 in the liquid phase measured by Capelli et al. [19] have not yet been incorporated in the model, and that the activities for other binary systems are not known. We trust this lack of data are the main reasons for the observed deviations.

Summing up single contributions to get total vapour pressure, we note a good agreement between calculations and the experimental values: using extrapolated values from equations in Table 2, the deviation is within 30% from 1000 to 1700 K. However, for higher temperatures, this deviation increases resulting in a significant difference in the boiling point, taken at 1 bar: the calculated value is 2014 K, while the value obtained from extrapolation of equations in Table 2 is 1908 ± 77 K. We note that the calculated value is outside the propagated uncertainty. This is due to the wide temperature range used for the extrapolation and to the vapour pressures of UF_4 and ThF_4, which are predicted to be higher and have a relatively steep slope. This significant deviation underlines the need to adjusts activities in the liquid phase in the thermodynamic model.

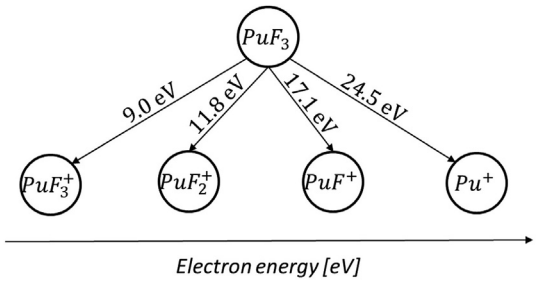

Fig. 5. Electron energies to create ions from a neutral PuF_3 precursor.

4. Conclusions

This work presents new measurements for PuF_3 and for the mixture LiF-ThF_4-UF_4-PuF_3 (77.5–6.6-12.3–3.6 mol%), selected as a possible fuel composition for the MSFR.

PuF_3 was assessed by KEMS and the following results are presented:

- melting point;

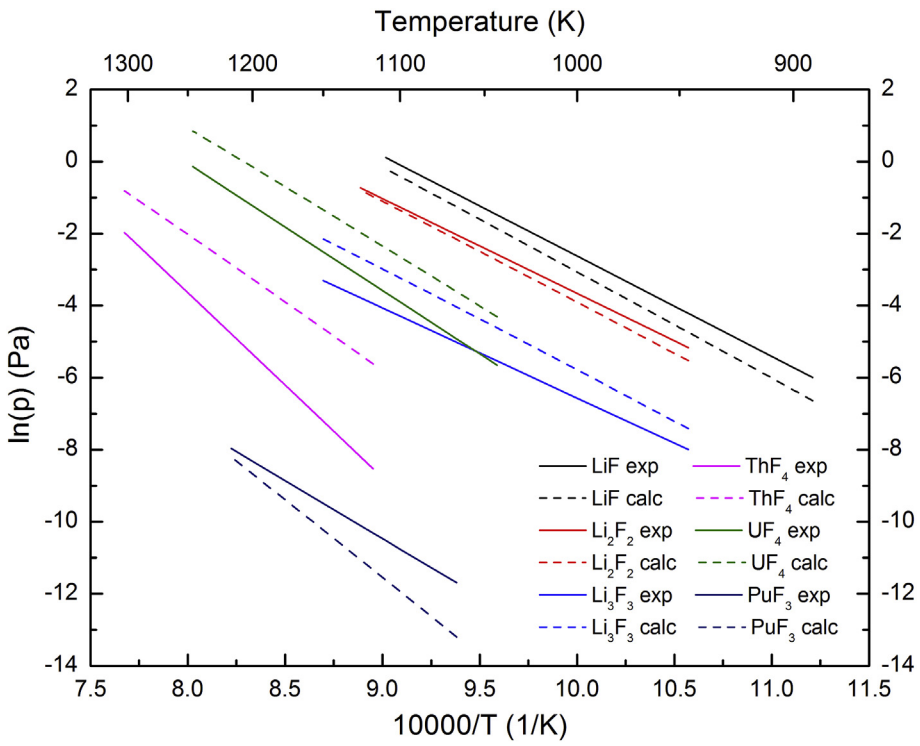

Fig. 7. Partial vapour pressures for the mixture LiF-ThF_4-UF_4-PuF_3 (77.5–6.6-12.3–3.6 mol%). Solid lines are linear fits of experimental values measured in this work. Dashed lines are calculated values using the thermodynamic database assessed by Capelli et al. [36].

Table 2
Partial vapour pressure formulas for the mixture LiF-ThF_4-UF_4-PuF_3 (77.5–6.6-12.3–3.6 mol%) and temperature ranges of validity.

Species	Equation	T range [K]
LiF(g)	$\ln p(\mathrm{Pa}) = -\frac{(27840\pm468)}{T(\mathrm{K})} + (25.214\pm0.432)$	892–1109
Li_2F_2(g)	$\ln p(\mathrm{Pa}) = -\frac{(26356\pm603)}{T(\mathrm{K})} + (22.693\pm0.706)$	946–1124
Li_3F_3(g)	$\ln p(\mathrm{Pa}) = -\frac{(24838\pm289)}{T(\mathrm{K})} + (18.010\pm0.538)$	946–1152
ThF_4(g)	$\ln p(\mathrm{Pa}) = -\frac{(51250\pm615)}{T(\mathrm{K})} + (37.360\pm0.559)$	1117–1043
UF_4(g)	$\ln p(\mathrm{Pa}) = -\frac{(35272\pm373)}{T(\mathrm{K})} + (28.168\pm0.526)$	1043–1246
PuF_3(g)	$\ln p(\mathrm{Pa}) = -\frac{(32199\pm479)}{T(\mathrm{K})} + (18.512\pm0.445)$	1066–1216

- equation describing vapour pressure vs. temperature valid for the range from 1310 to 1629 K;
- enthalpy of sublimation based on second and third law treatment of experimental values;
- ionization energies by electron impact from the neutral PuF_3 precursor.

These properties were previously assessed by other authors [38–41] and this work basically confirms literature results and provides a second independent study.

The mixture LiF-ThF_4-UF_4-PuF_3 (77.5–6.6-12.3–3.6 mol%) was assessed by DSC and KEMS, and the following results are presented:

- eutectic melting and liquidus point measured by DSC;
- equations describing partial vapour pressures vs. temperature for all species in ranges from 892 to 1216 K;
- boiling point determined by extrapolation of the vapour pressure data up to 1 bar.

Because no experimental data was available in literature for this mixture, results were discussed comparing calculated values obtained using the thermodynamic database assessed by Capelli et al. [36]. In general, calculations predicted quite well experimental values, but some significant deviations (e.g. in the boiling point) suggest slight modifications in the thermodynamic functions.

The results presented in this work aim to support the safety assessment of the MSFR. In this regard, the equations describing partial vapour pressures may be used to predict consequences due to the evaporation of the fuel. The low total vapour pressure and the high boiling point of the selected mixture confirm important safety features for this reactor concept.

Data availability

The raw/processed data required to reproduce these findings are available on request.

Acknowledgements

This work was funded by the Euratom research and training programme 2014-2018 under grant agreement No 661891 (SAMOFAR).

Alberto Tosolin would like to thank his current employer Canadian Nuclear Laboratories (CNL) for the courtesy extended, allowing him to finish this article.

Annex Tables

Annex Table 1
Vapour pressure results of PuF_3 obtained by KEMS in this work.

T [K]	*p* [Pa]	*T* [K]	*p* [Pa]	*T* [K]	*p* [Pa]	*T* [K]	*p* [Pa]
1309.6	2.51E-02	1395.5	2.31E-01	1477.6	1.47E+00	1559.9	7.15E+00
1313.0	2.55E-02	1399.0	2.43E-01	1480.9	1.56E+00	1563.3	7.60E+00
1316.1	2.96E-02	1402.2	2.78E-01	1484.4	1.68E+00	1566.4	8.04E+00
1319.7	3.08E-02	1405.6	2.94E-01	1487.5	1.78E+00	1569.4	8.52E+00
1322.9	3.47E-02	1409.0	3.17E-01	1490.7	1.92E+00	1572.8	9.09E+00
1326.6	3.95E-02	1412.1	3.41E-01	1494.3	2.03E+00	1576.3	9.59E+00
1329.8	4.73E-02	1415.5	3.68E-01	1497.5	2.19E+00	1579.4	1.02E+01
1333.3	4.74E-02	1419.0	3.97E-01	1501.0	2.32E+00	1582.8	1.08E+01
1336.9	5.09E-02	1422.1	4.31E-01	1504.2	2.47E+00	1585.8	1.14E+01
1340.2	5.44E-02	1425.6	4.64E-01	1507.3	2.65E+00	1588.4	1.20E+01
1343.6	6.05E-02	1428.9	5.01E-01	1510.8	2.81E+00	1590.7	1.26E+01
1346.9	6.70E-02	1432.5	5.40E-01	1514.0	3.02E+00	1593.4	1.31E+01
1350.7	7.52E-02	1435.6	5.87E-01	1517.7	3.22E+00	1596.2	1.37E+01
1354.1	8.02E-02	1438.9	6.28E-01	1520.7	3.43E+00	1599.1	1.44E+01
1357.4	8.80E-02	1441.9	6.70E-01	1523.9	3.65E+00	1602.1	1.51E+01
1361.1	9.83E-02	1445.1	7.17E-01	1527.3	3.87E+00	1604.6	1.58E+01
1364.4	1.07E-01	1447.8	7.70E-01	1530.7	4.15E+00	1607.7	1.70E+01
1367.9	1.17E-01	1451.2	8.22E-01	1533.8	4.40E+00	1610.8	1.78E+01
1371.4	1.25E-01	1454.5	8.79E-01	1537.0	4.69E+00	1613.5	1.87E+01
1374.7	1.42E-01	1457.3	9.48E-01	1540.1	4.98E+00	1616.5	1.97E+01
1378.3	1.53E-01	1460.8	1.03E+00	1543.7	5.29E+00	1619.9	2.06E+01
1381.8	1.66E-01	1464.3	1.11E+00	1546.8	5.61E+00	1622.8	2.16E+01
1385.2	1.80E-01	1467.7	1.17E+00	1550.0	5.96E+00	1625.9	2.28E+01
1388.6	1.96E-01	1471.2	1.26E+00	1553.4	6.33E+00	1628.6	2.39E+01
1391.9	2.17E-01	1474.4	1.36E+00	1556.6	6.75E+00		

Annex Table 2
Partial vapour pressure results of lithium fluoride species, ThF_4, UF_4 and PuF_3 in the mixture LiF-ThF_4-UF_4-PuF_3 (77.5−6.6-12.3−3.6 mol%).

T [K]	p(LiF) [Pa]	T [K]	p(Li_2F_2) [Pa]	T [K]	p(Li_3F_3) [Pa]	T [K]	p(ThF_4) [Pa]	T [K]	p(UF_4) [Pa]	T [K]	p(PuF_3) [Pa]
892	2.86E-03	945.7	5.41E-03	945.7	2.70E-04	1117.3	2.02E-04	1043.4	3.24E-03	1066	9.12E-06
900.5	3.22E-03	953	7.13E-03	953	3.35E-04	1122.6	2.16E-04	1048.9	3.85E-03	1076.7	1.04E-05
908.8	4.39E-03	959.5	8.37E-03	959.5	3.60E-04	1127.6	2.67E-04	1054.5	5.17E-03	1092.5	1.60E-05
916.5	5.62E-03	966	9.77E-03	966	4.22E-04	1133.3	4.60E-04	1059.9	5.72E-03	1097.7	2.57E-05
923.9	6.69E-03	972.1	1.13E-02	972.1	5.01E-04	1138.5	4.24E-04	1065.1	6.87E-03	1108.1	2.50E-05
931.2	9.27E-03	977.8	1.33E-02	977.8	6.11E-04	1143.6	7.94E-04	1070.6	8.39E-03	1113.1	2.59E-05
938.5	1.16E-02	983.6	1.59E-02	983.6	7.06E-04	1148.8	8.49E-04	1075.9	9.83E-03	1118.4	3.59E-05
945.7	1.42E-02	988.9	1.87E-02	988.9	8.24E-04	1155	8.62E-04	1081.4	1.11E-02	1133.9	4.97E-05
953	1.74E-02	994.4	2.18E-02	994.4	9.60E-04	1159.7	1.03E-03	1086.9	1.39E-02	1160.5	8.93E-05
959.5	2.13E-02	999.4	2.56E-02	999.4	1.06E-03	1164.9	1.23E-03	1091.9	1.63E-02	1166	1.12E-04
966	2.60E-02	1004.5	2.98E-02	1004.5	1.18E-03	1169.9	1.40E-03	1097.2	1.90E-02	1171	1.28E-04
972.1	3.13E-02	1009.4	3.37E-02	1009.4	1.40E-03	1175.3	1.98E-03	1102.3	2.24E-02	1175.8	2.13E-04
977.8	3.69E-02	1014.2	3.90E-02	1014.2	1.54E-03	1180.4	2.28E-03	1107.6	2.62E-02	1181.3	1.06E-04
983.6	4.38E-02	1020.2	4.44E-02	1020.2	1.81E-03	1185.4	2.83E-03	1112.4	3.10E-02	1186.4	1.76E-04
988.9	5.30E-02	1026.8	5.21E-02	1026.8	2.05E-03	1190.7	3.39E-03	1117.4	3.56E-02	1191.4	2.03E-04
994.4	6.26E-02	1033.5	6.26E-02	1033.5	2.46E-03	1195.7	4.10E-03	1122.9	4.18E-02	1196.5	2.01E-04
999.4	7.41E-02	1039.4	7.19E-02	1039.5	2.83E-03	1200.5	4.81E-03	1127.8	4.74E-02	1206.4	2.66E-04
1004.5	8.52E-02	1045.1	8.50E-02	1045.1	3.30E-03	1205.5	5.71E-03	1133.3	5.44E-02	1211.4	3.64E-04
1009.4	9.89E-02	1050.9	9.60E-02	1050.9	3.65E-03	1210.3	7.00E-03	1138.6	6.38E-02	1216.4	3.81E-04
1014.2	1.15E-01	1056.3	1.09E-01	1056.3	4.14E-03	1215.4	8.42E-03	1143.7	7.24E-02		
1020.2	1.34E-01	1061.5	1.23E-01	1061.5	4.74E-03	1220.7	9.85E-03	1149	8.42E-02		
1026.8	1.58E-01	1067.1	1.39E-01	1067.1	5.18E-03	1225.9	1.18E-02	1155.2	9.56E-02		
1033.5	1.84E-01	1072.5	1.55E-01	1072.5	5.84E-03	1230.7	1.35E-02	1159.8	1.08E-01		
1039.4	2.16E-01	1077.7	1.73E-01	1077.7	6.38E-03	1235.8	1.62E-02	1165	1.24E-01		
1045.1	2.54E-01	1083.1	1.94E-01	1083.1	7.30E-03	1240.5	1.91E-02	1170.1	1.39E-01		
1050.9	2.88E-01	1088.5	2.17E-01	1088.5	8.09E-03	1245.6	2.25E-02	1175.3	1.57E-01		
1056.3	3.30E-01	1093.6	2.45E-01	1093.6	9.40E-03	1250.6	2.63E-02	1180.5	1.76E-01		
1061.5	3.75E-01	1098.9	2.71E-01	1098.9	9.96E-03	1255.5	3.04E-02	1185.7	1.99E-01		
1067.1	4.22E-01	1104.1	3.00E-01	1104.1	1.12E-02	1260.7	3.58E-02	1190.8	2.24E-01		
1072.5	4.73E-01	1109.2	3.31E-01	1109.2	1.25E-02	1265.5	4.31E-02	1195.7	2.54E-01		
1077.7	5.35E-01	1114.4	3.68E-01	1114.4	1.39E-02	1270.6	5.04E-02	1200.6	2.85E-01		
1083.1	6.06E-01	1119.3	4.04E-01	1119.3	1.51E-02	1275.3	5.97E-02	1205.7	3.22E-01		
1088.5	6.79E-01	1124.6	4.46E-01	1124.6	1.70E-02	1279.8	7.00E-02	1210.6	3.68E-01		
1093.6	7.59E-01			1130.2	1.87E-02	1284.7	8.03E-02	1215.7	4.15E-01		
1098.9	8.46E-01			1135.2	2.06E-02	1289.2	9.30E-02	1220.8	4.73E-01		
1104.1	9.46E-01			1140.4	2.32E-02	1294	1.07E-01	1226	5.37E-01		
1109.2	1.04E+00			1145.5	2.50E-02	1298.5	1.22E-01	1230.8	6.04E-01		
				1151.5	2.77E-02	1303.1	1.41E-01	1236	6.85E-01		
								1240.8	7.75E-01		
								1245.9	8.76E-01		

References

[1] E.S. Bettis, R.W. Schroeder, G.A. Cristy, H.W. Savage, R.G. Affel, L.F. Hemphill, The aircraft reactor experiment-design and construction 1, Nucl. Sci. Eng. 2 (1957) 804–825, https://doi.org/10.13182/NSE57-A35495.

[2] E.S. Bettis, W.B. Cottrell, E.R. Mann, J.L. Meem, G.D. Whitman, The aircraft reactor experiment—operation, Nucl. Sci. Eng. 2 (1957) 841–853, https://doi.org/10.13182/NSE57-A35497.

[3] P.N. Haubenreich, J.R. Engel, Experience with molten-salt reactor experiment, Nucl. Appl. Technol. 8 (1970) 118–136, https://doi.org/10.13182/nt8-2-118.

[4] E.S. Bettis, R.C. Robertson, The design and performance features of a single-fluid molten-salt breeder reactor, Nucl. Appl. Technol. 8 (1970) 190–207, https://doi.org/10.13182/NT70-A28625.

[5] R.C. Robertson, O.L. Smith, R.B. Briggs, E.S. Bettis, Two-fluids molten-salt breeder reactor design study, ORNL-4528 (1970), https://doi.org/10.2172/4093364.

[6] H.G. MacPherson, The molten salt reactor adventure, Nucl. Sci. Eng. 90 (1985) 374–380, https://doi.org/10.13182/NSE90-374.

[7] OECD Nuclear Energy Agency, Technology Roadmap Update for Generation IV Nuclear Energy Systems, 2014, pp. 1–66. https://www.gen-4.org/gif/upload/docs/application/pdf/2014-03/gif-tru2014.pdf.

[8] J. Serp, M. Allibert, O. Beneš, S. Delpech, O. Feynberg, V. Ghetta, D. Heuer, D. Holcomb, V. Ignatiev, J.L. Kloosterman, L. Luzzi, E. Merle-Lucotte, J. Uhlíř, R. Yoshioka, D. Zhimin, The molten salt reactor (MSR) in generation IV: overview and perspectives, Prog. Nucl. Energy 77 (2014) 308–319, https://doi.org/10.1016/j.pnucene.2014.02.014.

[9] T.J. Dolan, Molten Salt Reactors and Thorium Energy, Woodhead Publishing, 2017.

[10] M. Allibert, M. Aufiero, M. Brovchenko, S. Delpech, V. Ghetta, D. Heuer, A. Laureau, E. Merle-Lucotte, Molten Salt Fast Reactors, 2016, https://doi.org/10.1016/B978-0-08-100149-3.00007-0.

[11] L. Mathieu, D. Heuer, E. Merle-Lucotte, R. Brissot, C. Le Brun, E. Liatard, J.-M. Loiseaux, O. Méplan, A. Nuttin, D. Lecarpentier, Possible configurations for the thorium molten salt reactor and advantages of the fast nonmoderated version, Nucl. Sci. Eng. 161 (2009) 78–89, https://doi.org/10.13182/NSE07-49.

[12] L. Luzzi, M. Aufiero, A. Cammi, C. Fiorina, March 14, in: Jinhai Zheng (Ed.), Thermo-Hydrodynamics of Internally Heated Molten Salts for Innovative Nuclear Reactors, Hydrodynamics - Theory and Model, IntechOpen, 2012, pp. 119–142, https://doi.org/10.5772/35924.

[13] J.L. Kloosterman, Safety assessment of the molten salt fast reactor (SAMOFAR) (Book Chapter), in: Molten Salt Reactors and Thorium Energy, June 2017, pp. 565–570 .

[14] M. Allibert, D. Gérardin, D. Heuer, E. Huffer, A. Laureau, E. Merle, S. Beils, A. Cammi, B. Carluec, S. Delpech, A. Gerber, E. Girardi, J. Krepel, D. Lathouwers, D. Lecarpentier, S. Lorenzi, L. Luzzi, M. Ricotti, V. Tiberi, SAMOFAR European Project D1.1 Description of Initial Reference Design and Identification of Safety Aspects, 2017. Contract number: 661891.

[15] S. Delpech, E. Merle-Lucotte, D. Heuer, M. Allibert, V. Ghetta, C. Le-Brun, X. Doligez, G. Picard, Reactor physic and reprocessing scheme for innovative molten salt reactor system, J. Fluorine Chem. 130 (2009) 11–17, https://doi.org/10.1016/j.jfluchem.2008.07.009.

[16] D. Heuer, E. Merle-Lucotte, M. Allibert, M. Brovchenko, V. Ghetta, P. Rubiolo, Towards the thorium fuel cycle with molten salt fast reactors, Ann. Nucl. Energy 64 (2014) 421–429, https://doi.org/10.1016/j.anucene.2013.08.002.

[17] A. Tosolin, O. Beneš, J.-Y. Colle, P. Souček, L. Luzzi, R.J.M. Konings, Vaporization behaviour of the molten salt fast reactor fuel: the LiF-ThF_4 -UF_4 system, J. Nucl. Mater. 508 (2018) 319–328, https://doi.org/10.1016/j.jnucmat.2018.05.049.

[18] E. Merle-Lucotte, D. Heuer, M. Allibert, X. Doligez, V. Ghetta, Optimizing the burning efficiency and the deployment capacities of the molten salt fast reactor, in: Global, 2009, pp. 1864–1872. Paris.

[19] E. Capelli, O. Beneš, J.-Y. Colle, R.J.M. Konings, Determination of the thermodynamic activities of LiF and ThF_4 in the Li_x Th_{1-x} F_{4-3x} liquid solution by Knudsen effusion mass spectrometry, Phys. Chem. Chem. Phys. 17 (2015) 30110–30118, https://doi.org/10.1039/C5CP04777C.

[20] P. Souček, O. Beneš, B. Claux, E. Capelli, M. Ougier, V. Tyrpekl, J.-F. Vigier, R.J.M. Konings, Synthesis of UF_4 and ThF_4 by HF gas fluorination and re-determination of the UF_4 melting point, J. Fluorine Chem. 200 (2017) 33–40, https://doi.org/10.1016/j.jfluchem.2017.05.011.

[21] A. Tosolin, P. Souček, O. Beneš, J.-F. Vigier, L. Luzzi, R.J.M. Konings, Synthesis of plutonium trifluoride by hydro-fluorination and novel thermodynamic data of PuF_3 -LiF system, J. Nucl. Mater. 503 (2018) 171–177, https://doi.org/10.1016/j.jnucmat.2018.02.037.

[22] S. Mukherjee, S. Dash, S.K. Mukerjee, K.L. Ramakumar, Thermodynamic investigations of oxyfluoride of thorium and uranium, J. Nucl. Mater. 465 (2015) 604–614, https://doi.org/10.1016/j.jnucmat.2015.06.038.

[23] C.J. Mandleberg, D. Davies, The reaction of UF_4 with oxygen, J. Inorg. Nucl. Chem. 20 (1961) 58–61, https://doi.org/10.1016/0022-1902(61)80458-2.

[24] R.B. Briggs, Molten-Salt Reactor Program Semiannual Progress Report for Period Ending July 31, 1964. ORNL-3708, 1964. http://technicalreports.ornl.gov/1964/3445600500358.pdf.

[25] O. Beneš, R.J.M. Konings, S. Wurzer, M. Sierig, A. Dockendorf, A DSC study of the $NaNO_3$-KNO_3 system using an innovative encapsulation technique, Thermochim. Acta 509 (2010) 62–66, https://doi.org/10.1016/j.tca.2010.06.003.

[26] J.-Y. Colle, D. Freis, O. Bene, R.J.M. Konings, Knudsen effusion mass spectrometry of nuclear materials: applications and developments, ECS Trans 46 (2013) 23–38, https://doi.org/10.1149/04601.0023ecst.

[27] K. Hilpert, High-temperature mass spectrometry in materials research, Rapid Commun. Mass Spectrom. 5 (1991) 175–187, https://doi.org/10.1002/rcm.1290050408.

[28] J. Drowart, C. Chatillon, J. Hastie, D. Bonnell, High-temperature mass spectrometry: instrumental techniques, ionization cross-sections, pressure measurements, and thermodynamic data (IUPAC Technical Report), Pure Appl. Chem. 77 (2005) 683–737, https://doi.org/10.1351/pac200577040683.

[29] D.R. Lide, S.R. Data, E.A. Board, G. Baysinger, S. Chemistry, C.E. Library, L.I. Berger, R.N. Goldberg, B. Division, H. V Kehiaian, K. Kuchitsu, G. Rosenblatt, D.L. Roth, D. Zwillinger, CRC Handbook of Chemistry and Physics, 2005. Internet Version, http://www.hbcpnetbase.com.

[30] R. Grimley, The Characterization of High Temperature Vapours, John Wiley and Sons, Inc., 1967.

[31] M. Yamawaki, M. Hirai, M. Yasumoto, M. Kanno, Mass spectrometric study of vaporization of lithium fluoride, J. Nucl. Sci. Technol. 19 (1982) 563–570.

[32] J.B. Mann, Ionization cross sections of the elements calculated from mean-square radii of atomic orbitals, J. Chem. Phys. 46 (1967) 1646, https://doi.org/10.1063/1.1840917.

[33] H. Deutsch, K. Becker, T.D. Märk, A modified additivity rule for the calculation of electron impact ionization cross-section of molecules AB_n, Int. J. Mass Spectrom. Ion Process. 167–168 (1997) 503–517, https://doi.org/10.1016/S0168-1176(97)00108-0.

[34] J.P. Desclaux, Relativistic Dirac-Fock expectation values for atomos with Z=1 to Z=120, Atomic Data Nucl. Data Tables 12 (1973) 311–406.

[35] G.W.H. Höhne, W. Hemminger, H.-J. Flammersheim, Differential Scanning Calorimetry, Springer Berlin Heidelberg, Berlin, Heidelberg, 1996, https://doi.org/10.1007/978-3-662-03302-9.

[36] E. Capelli, O. Beneš, R.J.M. Konings, Thermodynamic assessment of the LiF-ThF_4-PuF_3-UF_4 system, J. Nucl. Mater. 462 (2015) 43–53, https://doi.org/10.1016/j.jnucmat.2015.03.042.

[37] C.W. Bale, E. Bélisle, P. Chartrand, S.A. Decterov, G. Eriksson, A.E. Gheribi, K. Hack, I.-H. Jung, Y.-B. Kang, J. Melançon, A.D. Pelton, S. Petersen, C. Robelin, J. Sangster, P. Spencer, M.-A. Van Ende, FactSage thermochemical software and databases, 2010–2016, Calphad 54 (2016) 35–53, https://doi.org/10.1016/j.calphad.2016.05.002.

[38] R.A. Kent, Mass spectrometric studies of plutonium compounds at high temperatures. II. Enthalpy of sublimation of plutonium(III) fluoride and the dissociation energy of plutonium(I) fluoride, J. Am. Chem. Soc. 90 (1968) 5657–5659, https://doi.org/10.1021/ja01023a002.

[39] E.F. Westrum, J.C. Wallmann, The melting point and the heat of sublimation of plutonium trifluoride 1, J. Am. Chem. Soc. 73 (1951) 3530–3531, https://doi.org/10.1021/ja01151a535.

[40] T.E. Phipps, G.W. Sears, R.L. Seifert, O.C. Simpson, The vapor pressure of plutonium halides, J. Chem. Phys. 18 (1950) 713–723, https://doi.org/10.1063/1.1747733.

[41] S.C. Carniglia, B.B. Cunningham, Vapor pressures of americium trifluoride and plutonium trifluoride, heats and free energies of sublimation, J. Am. Chem. Soc. 77 (1955) 1451–1453, https://doi.org/10.1021/ja01611a015.

[42] R.J. Lemire, J. Fuger, N. Heino, P. Paul, M.H. Rand, J. Rydberg, K. Spahiu, J. Sullivan, W.J. Ullman, P. Vitorge, H. Wanner, Chemical Thermodynamich of Neptunium and Plutonium, Elsevier, 2001.